AGU PUBLICATIONS

JGR

Journal of Geophysical Research: Biogeosciences

RESEARCH ARTICLE
10.1002/2013JG002596

Key Points:
- A two-leaf rectangular hyperbolic model (RHM) for GPP estimation was developed
- The two parameters of the modified RHM vary with temperature and vegetation type
- RHM has the potentials of simplicity as LUE model and accuracy as process model

Correspondence to:
F. Wang,
wfmwfmwfmwfm@163.com

Citation:
Wang, F., J. M. Chen, A. Gonsamo, B. Zhou, F. Cao, and Q. Yi (2014), A two-leaf rectangular hyperbolic model for estimating GPP across vegetation types and climate conditions, *J. Geophys. Res. Biogeosci.*, *119*, 1385–1398, doi:10.1002/2013JG002596.

Received 13 DEC 2013
Accepted 2 JUL 2014
Accepted article online 7 JUL 2014
Published online 24 JUL 2014

A two-leaf rectangular hyperbolic model for estimating GPP across vegetation types and climate conditions

Fumin Wang[1], Jing M. Chen[2], Alemu Gonsamo[2], Bin Zhou[3], Feifeng Cao[4], and Qiuxiang Yi[5]

[1]Institute of Hydrology and Water Resources, Zhejiang University, Hangzhou, China, [2]Department of Geography and Program in Planning, University of Toronto, Toronto, Ontario, Canada, [3]Institute of Remote Sensing and Earth Sciences, Hangzhou Normal University, Hangzhou, China, [4]Institute of Harbor-Channel and Coastal Engineering, Department of Civil Engineering, Zhejiang University of Technology, Hangzhou, China, [5]Xinjiang Institute of Ecology and Geography, Chinese Academy of Sciences, Xinjiang, China

Abstract There are mainly three types of gross primary production (GPP), including light use efficiency (LUE) model, rectangular hyperbolic model (RHM), and process-based model (PBM). RHM is not widely used because its parameters, namely, quantum yield (α) and maximum photosynthetic rate (P_m), vary temporally with temperature and spatially with vegetation type under natural conditions. In the study, we present a temperature- and vegetation-type-adapted RHM by linking it to the Baldocchi's model to obtain the relationship between α-P_m and $V_{cmax,25}$-temperature to overcome the shortcomings of traditional RHM. The modified RHM (MRHM) coupled with a two-leaf upscaling strategy makes it possible to accurate and fast estimation of GPP at large scale. Twenty-two CO_2 eddy-covariance sites with different vegetation types, including evergreen needleleaf forest, deciduous broadleaf forest, grassland, and evergreen broadleaf forest, are used to evaluate the performance of MRHM for GPP estimation. The comparisons of the simulated GPP using MRHM with measured and Boreal Ecosystem Productivity Simulator-simulated GPP demonstrate that the MRHM can simulate GPP as accurately as PBM and in the meantime with the advantage of simplicity as LUE model. These results show the promising potential of MRHM for accurately simulating GPP with relative high computational efficiency, providing an ideal alternative tool for large-scale and long time series GPP simulations.

1. Introduction

Gross primary production (GPP), defined as the overall photosynthetic fixation of carbon per unit space and time, plays a key role in understanding the carbon balance between the biosphere and atmosphere [*Yang et al*., 2013]. Global estimation and monitoring of GPP is critical for climate change research [*Hilker et al*., 2008]. Although flux networks with more than 500 towers covering a wide range of biomes have been set up across the globe to continually measure the dynamics of CO2 flux [*Law et al*., 2000; *Baldocchi et al*., 2001], each site represents a small area with records available for only a limited period [*Coops et al*., 2009]. So the modeling of GPP is still a primary way to study ecosystem carbon balance at landscape, regional, and global scales. During recent decades, a wide variety of models have been used to estimate GPP, these models can be classified into three broad categories: Light use efficiency (LUE) model, hyperbolic model, and process-based model.

The LUE concept was initially proposed by *Monteith* [1972], who stated that carbon fixation is a function of the incident photosynthetically active radiation absorbed by vegetation (APAR) and LUE (ε) which represents the conversion efficiency of APAR. From then, a variety of LUE models were developed based on the LUE concept [*Potter et al*., 1993; *Prince and Goward*, 1995; *Xiao et al*., 2005; *Yang et al*., 2013]. The ε is a key variable to be determined in LUE models. It is often expressed as biome-specific constants, adjusted through globally measurable meteorological variables representing canopy stresses, such as temperature and vapor pressure deficit, and soil water content [*Running et al*., 2004]. A LUE model has the advantage of simplicity, and it can be easily coupled with the remote sensing data to approximately address the spatial and temporal dynamics of GPP. However, since it usually uses big-leaf strategy for spatial upscaling and multiday average for temporal upscaling, the reliability of this approach in assessing GPP, in particular for spatial and temporal scales beyond those used to derive the empirical relationships, has been questioned [*Zhang et al*., 2012] due to the trade-off between ease of use and accuracy.

Recent years, process-based models (PBM) have been widely used to simulate GPP at hourly to daily time steps. PBM usually involves the mechanistic processes of photosynthesis, as described in the Farquhar's model [*Farquhar et al*., 1980] and its variants [*Baldocchi*, 1994]. In these models, the maximum carboxilation rate at 25C° ($V_{cmax,25}$) is an important parameter, which determines the maximum carboxylation capacity for a specific biome and is assumed to be a fixed value for each vegetation type. In general, PBMs are considered to perform better than LUE models [*Zhang et al*., 2012], but PBMs have the disadvantage of complexity because the large number of model parameters involved in these models result in a laborious and time-consuming computation demand as well as the need to compile a large input data set, some of which may not be available. Although these parameters are interpreted as being physically and biologically meaningful, they greatly lower the computation efficiency.

Since the territorial carbon flux is so important in the global carbon cycle affecting the climate, there is a strong need to estimate the carbon flux across spatial and temporal scales. Therefore, a model with both high accuracy and computation efficiency is highly desirable for the purpose of producing long time series of GPP at high spatial resolutions. Hyperbolic models (HM) have the potential to achieve this goal. HMs are empirical models with simple forms, including rectangular hyperbolic models (HRM) [*Saito et al*., 2005; *Xiao*, 2006; *Kanniah et al*., 2013] and nonrectangular hyperbolic models (NHRM) [*Ide et al*., 2010]; both types have the same two key parameters, namely, maximum photosynthetic rate at light saturation (P_m) and apparent quantum yield (α) defined as the initial slope of the light response curve [*Xiao et al*., 2005; *Yan et al*., 2009]. The hyperbolic models have the potential to simulate GPP as well as PBMs [*Pachepsky et al*., 1996] and have been shown to accurately simulate GPP at leaf level [*Pachepsky et al*., 1996] and canopy level [*Yan et al*., 2009]. HMs and PBMs are also generally used as an effective method to fill gaps for missing values of net ecosystem CO_2 exchange across CO_2 eddy-covariance tower sites. However, compared to LUE models and PBMs, HMs are rarely used in long-term large-scale GPP estimations because the two key parameters of HMs vary with temperature and vegetation type or biome. To avoid the strong dependence of the two parameters on temperature, previous studies applied HMs in temperature controlled experiments [*Pachepsky et al*., 1996; *Whitehead and Gower*, 2001] or in a short period of time such as a week or 10 days [*Suyker et al*., 2004; *Saito et al*., 2005; *Yan et al*., 2009], in which temperature was assumed to be invariant, to mitigate the seasonal effects [*Ide et al*., 2010]. To our knowledge, no effort has been made to simultaneously take temperature and vegetation type into account in a hyperbolic model for GPP estimation. And how temperature and vegetation type affect the two parameters of hyperbolic models remains unknown. Therefore, the objectives of this study are (1) to present a modified leaf-level RHM by establishing the relationships between the two parameters of RHM and temperature -$V_{cmax,25}$ of PBM and (2) subsequently to upscale the estimated leaf-level GPP to canopy level using a two-leaf upscaling strategy to estimate canopy GPP for different vegetation types. The overall goal of this study is to develop a new method for fast and accurate simulation of GPP, which has the advantage of similar simplicity to LUE models and accuracy to PBM. In this study, eddy-covariance measurements of CO_2 and the concurrent measurements of meteorological variables at 22 sites will be used to test the performance of modified RHM across different environmental condition and biomes.

2. Methodology

2.1. Description of Site and Data

The eddy-covariance (EC) data used here were downloaded directly from the AmeriFlux website (http://ameriflux.ornl.gov) and the Canadian Carbon Program (CCP) website (http://fluxnet.ccrp.ec.gc.ca), including 18 AmeriFlux sites and four Canadian sites, and the vegetation types include evergreen forests, deciduous forests, and grasslands. These sites were selected based on the availability of key data sets such as leaf area index (LAI), meteorology, and land surface C fluxes. To evaluate model performance with independent data, all sites for each vegetation type were separated as calibration and validation data sets. For every vegetation type, almost half of the sites are used for calibration, and the remaining sites are used for validation. A complete list of these sites is given in Table 1.

At each site, global radiation or photosynthetically active radiation (PAR), precipitation, air temperature, relative humidity, wind speed, and the CO_2 flux were measured on a half-hourly basis. Net ecosystem productivity (NEP) was calculated as NEP = −NEE, and GPP was calculated as the sum of daytime NEP and daytime ecosystem respiration. Besides, data gaps of the half-hourly GPP associated with equipment failures or unsuitable micrometeorological conditions were filled using the Artificial Neural Network (ANN) method [*Papale and Valentini*, 2003] or Barr's gap-filling method [*Barr et al*., 2004].

Table 1. The Description of Sites Used in This Study

Vegetation Type	Site ID	Longitude	Latitude	Year	Category	References
Evergreen needleleaf forest	US_NR1	−105.546	40.033	2005	Calibration	*Monson et al.* [2005]
	US_Ho2	−68.747	45.209	2004	Calibration	*Richardson and Hollinger* [2005]
	Ca_DF49	−125.335	49.869	2008	Calibration	*Jassal et al.* [2009]
	US_Ho1	−68.740	45.204	2004	Validation	*Hollinger et al.* [2004]
	US_Wrc	−121.952	45.821	2004	Validation	*Falk et al.* [2008]
	Ca_DF88	−124.900	49.535	2008	Validation	*Chen et al.* [2009]
	Ca_ HBS75	−74.571	49.760	2008	Validation	*Payeur-Poirier et al.* [2012]
Deciduous broadleaf forest	US_MOz	−92.200	38.744	2007	Calibration	*Gu et al.* [2007]
	US_MMS	−86.413	39.323	2004	Calibration	*Schmid et al.* [2000]
	Ca_OA	−106.198	53.629	2008	Calibration	*Barr et al.* [2004]
	US_Bar	−71.288	44.065	2006	Validation	*Jenkins et al.* [2007]
	US_Ha1_	−72.172	42.538	2004	Validation	*Urbanski et al.* [2007]
	US_UMB	−84.714	45.560	2004	Validation	*Curtis et al.* [2002]
	US_WCr	−90.080	45.806	2004	Validation	*Cook et al.* [2004]
Grassland	US_Var	−120.951	38.407	2005	Calibration	*Baldocchi* [2003]
	US_Aud	−110.509	31.591	2005	Calibration	*Krishnan et al.* [2012]
	US_Goo	−89.874	34.255	2004	Calibration	*Wilson and Meyers* [2007]
	US_Dk1	−79.093	35.971	2001	Validation	*Oren et al.* [2006]
	US_Fwf	−111.772	35.445	2007	Validation	*Dore et al.* [2010]
	US_IB2	−88.241	41.841	2006	Validation	*Allison et al.* [2005]
Evergreen broadleaf forest	BR_Sa1	−54.959	−2.857	2004	Calibration	*Wick et al.* [2005]
	BR_Sa3	−54.9714	−3.018	2002	Validation	*Goulden et al.* [2006]

2.2. A Modified Canopy-Level Rectangular Hyperbolic Model

2.2.1. Leaf-Level $V_{cmax,25}$-Temperature and α-P_m Relationship

The relationship between α-P_m and $V_{cmax,25}$-temperature is established through linking the *Baldocchi*'s [1994] model and hyperbolic model using a regression technique. The procedure is described in detail as follows:

First, a series of GPPs are calculated using Baldocchi's photosynthesis model with a series of photosynthetic photo flux density (PPFD) values as inputs for a combination of fixed temperature and $V_{cmax,25}$. In the Baldocchi's model, CO_2 concentration is set to 380 ppm, and the leaf boundary layer conductance to CO_2 is set to 1/48 m s^{-1}.

Second, we regress PPFD on GPP to fit a rectangular hyperbolic model for a given combination between temperature and $V_{cmax,25}$ to obtain the optimal two parameters of the rectangular hyperbolic model, α, P_m.

Finally, we repeat the above procedures for all the combinations of temperature from 1°C to 40°C and $V_{cmax,25}$ from 20 to 180 μmol m^{-2} s^{-1} to obtain a matrix of α and P_m.

A number of experiments have proved that RHM can better describe response of GPP to radiation at a constant temperature [*Pachepsky et al.*, 1996]. So good regression results can be expected. Figure 1 shows the R^2 of all fitted RHM for all combinations between temperature and $V_{cmax,25}$. Because there are two variables, temperature and $V_{cmax,25}$, all the R^2 values construct a matrix, called R^2 distribution map. Similarly, we can also get the α and P_m distribution map shown in the results section. As shown in Figure 1, when the R^2 values close to 1, the minimum value of R^2 distribution map occurring at the highest temperature and the largest $V_{cmax,25}$ value. This result indicates that modified rectangular hyperbolic model (MRHM) can track the GPP response to PPFD as good as mechanistic process-based model and can further expect the outstanding performance of MRHM to simulate response of GPP to radiation for a fixed temperature.

2.2.2. A Leaf-Level Temperature- and $V_{cmax,25}$-Adapted Rectangular Hyperbolic Model

Since the two parameters, α and P_m, of MRHM can be dynamically determined according to the values of temperature and $V_{cmax,25}$, they can be used in MRHM to model GPP under different radiation and temperature conditions. The leaf-level temperature-adapted gross carbon assimilation can be calculated as follows:

$$GCA_{leaf}\left(V_{cmax,25},T\right)=\frac{\alpha\left(V_{cmax,25},T\right)\times P_m\left(V_{cmax,25},T\right)\times APAR}{P_m\left(V_{cmax,25},T\right)+\alpha\left(V_{cmax,25},T\right)\times APAR}$$

where GCA_{leaf} is the leaf-level gross carbon assimilation at temperature T for a vegetation type with a fixed $V_{cmax,25}$, α, and P_m are the quantum yield and the maximum photosynthetic rate at light saturation condition,

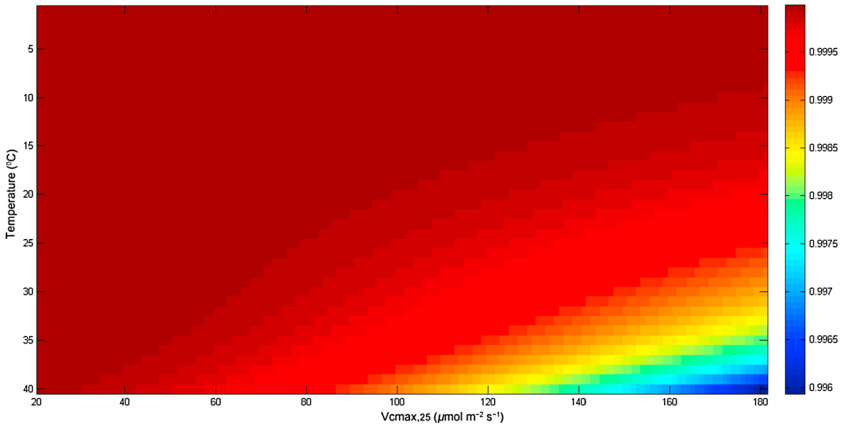

Figure 1. R^2 distribution map of rectangular hyperbolic models for different temperatures and $V_{cmax,25}$.

varying with temperature T and $V_{cmax,25}$. In the above equation, APAR instead of incident or intercepted PAR is used because that leaves respond to absorbed radiation, not incident or intercepted radiation.

Compared to traditional RHMs which usually treat α and P_m as a constant for a period of time or entire growing season, the proposed MRHM not only responds to radiation variation but also to temperature variation for a given vegetation type. So in this way, the shortcoming of traditional hyperbolic model is solved, and it can be used to accurately estimate GCA of vegetation across vast temporal and spatial scales. Since we do not consider the effect of relative humidity when establishing the leaf-level relationship between $V_{cmax,25}$-temperature and α-P_m, a scalar of vapor pressure deficit (VPD), f(VPD), is used to downregulate the GCA in MRHM under unfavorable conditions of high VPD, which make the temperature- and $V_{cmax,25}$-adapted RHM suitable for more environmental conditions.

$$GCA_{actual} = GCA_{leaf} \times f(VPD)$$

where the GCA_{actual} is GCA adjusted by VPD. And the f(VPD) is calculated as follows:

$$f(VPD) = \begin{cases} 0 & VPD \geq VPD_{max} \\ \dfrac{VPD_{max} - VPD}{VPD_{max} - VPD_{min}} & VPD_{min} \leq VPD \leq VPD_{max} \\ 1 & VPD \leq VPD_{min} \end{cases}$$

where VPD_{max}, VPD_{min} are the parameters dependent on vegetation types (Table 2).

2.2.3. Two-Leaf Upscaling Strategy From Leaf Level to Canopy Level

The canopy-level GPP (GPP_{canopy}) can be obtained as the sum of the total GPP of sunlit and shaded leaf groups [*Chen et al.*, 1999, 2012]:$GPP_{canopy} = GCA_{sunlit} \times LAI_{sunlit} + GCA_{shaded} \times LAI_{shaded}$where the subscripts "sunlit" and "shaded" denote the sunlit and shaded components of GCA and leaf area index (LAI). This two-leaf formulation is based on the estimation of the GCA of a representative sunlit leaf (GCA_{sunlit}) and a representative shaded leaf (GCA_{shaded}). The GCA_{sunlit} and GCA_{shaded} are calculated using the above

Table 2. Parameters Used for MRHM and BEPS[a]

Parameters	Unit	ENF	DBF	GRA	EBF	References
$V_{cmax,25}$	μmol m^{-2} s^{-1}	55	63	90	30	*Kattge et al.* [2009]; *Groenendijk et al.* [2011]
Ω	/	0.5	0.8	0.95	0.85	*Liu et al.* [1997]; *Chen et al.* [2012]
m	/	8	8	8	8	*Ball* [1988]; *Leuning et al.* [1995]
b	mol m^{-2} s^{-1}	0.0011	0.0011	0.0011	0.0011	*Ball* [1988]; *Leuning et al.* [1995]
VPD_{max},	pa	4100	4100	4100	4100	*He et al.* [2013]
VPD_{min}	pa	930	930	930	930	*He et al.* [2013]

[a]ENF: evergreen needleleaf forest, DBF: deciduous broadleaf forest, GRA: grassland, and EBF: evergreen broadleaf forest.

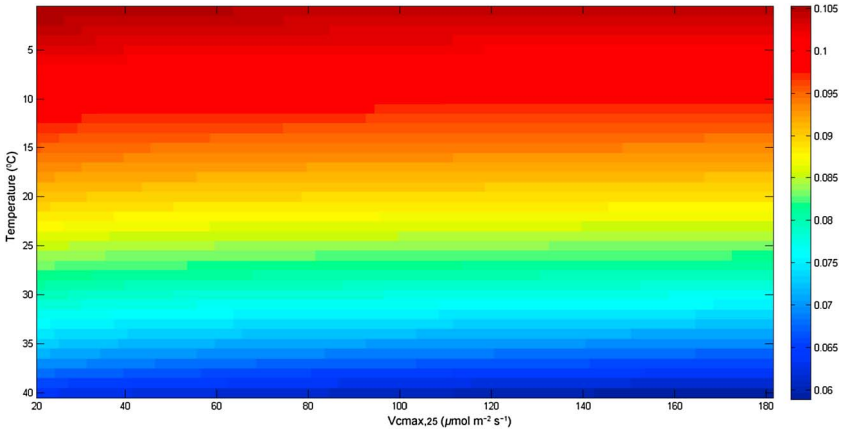

Figure 2. Quantum yield (α) distribution map for different air temperatures and $V_{cmax,25}$.

temperature- and $V_{cmax,25}$-adapted RHM. The APAR of sunlit and shaded leaves for the temperature- and $V_{cmax,25}$-adapted RHM are calculated using the methods of *Chen et al*. [1999].

The total LAI is separated into sunlit and shaded LAI using the original formulation of *Norman* [1982] with consideration of a foliage clumping index proposed by *Chen et al*. [1999] and assuming the canopy being spherical leaf angle distribution:

$$\mathrm{LAI}_{\mathrm{sunlit}} = 2\cos\theta\left(1 - e^{-0.5\Omega\mathrm{LAI}/\cos\theta}\right)$$

$$\mathrm{LAI}_{\mathrm{shaded}} = \mathrm{LAI} - \mathrm{LAI}_{\mathrm{sunlit}}$$

where θ is the solar zenith angle and Ω is the clumping index which characterizes the leaf spatial distribution pattern in terms of the degree of its deviation from the random case and influences radiation interception by the canopy at a given θ as described by Beer's law. The typical values of Ω are 0.5–0.7 for conifer forests and 0.7–0.9 for broadleaf forests [*Liu et al*., 1997; *Chen et al*., 1999]. For dense grass and shrub, Ω is found to be close to unity [*Liu et al*., 1997].

2.3. Model Evaluation and Intercomparison

Eddy-covariance (EC) measurements of CO_2 fluxes made at sites in Table 1 are used to evaluate the performance of MRHM. The half-hourly measurements are first summed to daily values, and then the daily values are used for model evaluation

The hourly Boreal Ecosystem Productivity Simulator (BEPS) [*Ju et al*., 2006; *Liu et al*., 1997] are also used for further intercomparison of MRHM. The BEPS model is a process-based ecosystem process model with a canopy energy balance module [*Chen et al*., 2007]. The GPP simulated by BEPS will be used as a standard data to compare with GPP simulated by MRHM. The key biochemical and biophysical parameters used for the four vegetation types in the hourly BEPS and MRHM are given in Table 2.

3. Results and Analysis

3.1. Relationship Between α and Temperature-Vegetation Type

3.1.1. Distribution Pattern of the α Map

By linking Baldocchi's photosynthesis model and RHM, we obtain the quantum yield distribution map with temperatures varying from 1°C to 40°C and $V_{cmax,25}$ from 20 to 180 μmol m^{-2} s^{-1} depending on vegetation types (Figure 2). It can be seen from Figure 2 that the α values range from 0.059 to 0.105 with an average of 0.868. The α values remain similar for different $V_{cmax,25}$ values while they decrease with increasing temperature for a given $V_{cmax,25}$. The lowest value of α occurs at the highest temperature, and the highest value occurs at the lowest temperature. After averaging the α over $V_{cmax,25}$, we find that the average α decrease monotonically with increasing temperature and the variation coefficient is very small with the maximum value being less than 2% (Figure 3), which further proves that α is independent of $V_{cmax,25}$.

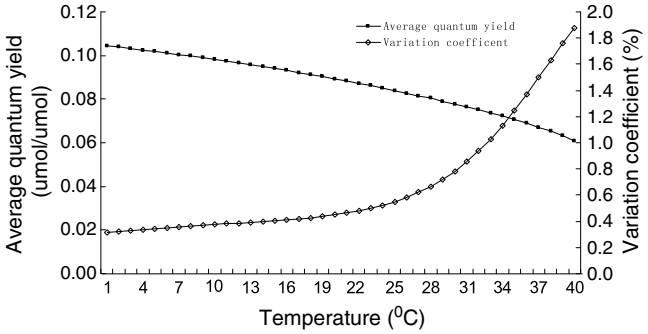

Figure 3. Variation of average quantum yield and its variation coefficient with temperature.

This indicates that the α is not be affected by vegetation types. Similar results have been reported by a number of literatures [*Sands*, 1995; *Saito et al*., 2005]. *Saito et al*. [2005] reported that the quantum yields obtained by fitted half-hourly GPP and APAR for six periods of a rice field varied from 0.109 to 0.046 for different growth stages, which had a similar variation range with that in our study. *Whitehead and Gower* [2001] compared α in a hyperbolic photosynthesis model for 11 species representing the dominant trees, understory shrubs, herbaceous plants and moss species in an old black spruce boreal forest ecosystem, and found that α values were similar for most species (0.078–0.080 μmol CO_2 μmol^{-1}), which is consistent with results from this study. *Vourlitis et al*. [2004] also found that quantum yields are relatively constant (0.07 μmol CO_2 μmol^{-1}) over seasonal time scales for a tropical forest eddy CO_2 flux station, that is because temperature variation is small for the tropical forest station.

3.1.2. Variations of α Across Vegetation Types

Following the variation ranges of $V_{cmax,25}$ from *Kattge et al*. [2009], we calculated the average and standard deviation (SD) of quantum yield among different vegetation types. Since the minimum temperature in tropical region usually is above 20°C, the α values under this condition are used to calculate average and SD values for tropical trees (Table 3). The differences in the average and SD of quantum yield are small for different vegetation types although they may have different leaf nitrogen contents. So, we can infer that α is independent of leaf nitrogen content, which is in agreement with *Sands* [1995]. The average α values are the same for the tropical trees (oxisols) and tropical trees (nonoxisols), so are SD values. Furthermore, the α and SD values are very similar to each other for the rest of vegetation types, and they are almost equal. The SD value of data per vegetation type is about 10–14% of the corresponding average, suggesting small variation of α relative to the large temperature variation range from 1 to 40°C.

3.2. Relationship Between P_m and Temperature-Vegetation Type

3.2.1. Distribution Pattern of the P_m Map

The P_m distribution map is determined in a similar ways as the quantum yield (α) map, which is shown in Figure 4. Compared to α, P_m varies not only with temperatures but also with vegetation types (i.e., $V_{cmax,25}$), ranging from 1.17 to 68.09 μmol m^{-2} s^{-1}. For a given $V_{cmax,25}$, P_m increases with increasing temperature from 1 to 25°C. The maximum P_m occurs at 25°C, and after then P_m decreases sharply with increasing temperature

Table 3. Average and Standard Deviation of Quantum Yield (α) and Maximum Photosynthetic Rate (P_m) Corresponding to Different Vegetation Types With Different $V_{cmax,25}$[a]

	$V_{cmax,25}$		α		P_m	
Vegetation Types	Avg	SD	Avg	SD	Avg	SD
Tropical trees (oxisols)	29.00	7.70	0.078	0.008	6.81	3.09
Tropical trees (nonoxisols)	41.00	15.10	0.078	0.008	10.28	4.91
Temperate evergreen broadleaf trees	61.40	27.70	0.087	0.012	13.84	7.35
Temperate deciduous broadleaf trees	57.70	21.20	0.087	0.012	12.99	6.51
Evergreen needleleaf trees	62.50	24.70	0.087	0.012	14.09	7.18
Deciduous needleleaf trees	39.10	11.70	0.088	0.012	8.31	4.09
Evergreen shrubs	61.70	24.60	0.087	0.012	13.84	7.09
Deciduous shrubs	54.00	14.50	0.087	0.012	12.14	5.73
C3 herbaceous	78.20	31.10	0.087	0.012	17.86	9.03
C3 crops	100.70	36.60	0.087	0.013	23.27	11.38

[a]Avg: average values; SD: standard deviation; oxisols or nonoxisols denotes that trees are grown on oxisols or nonoxisol soils.

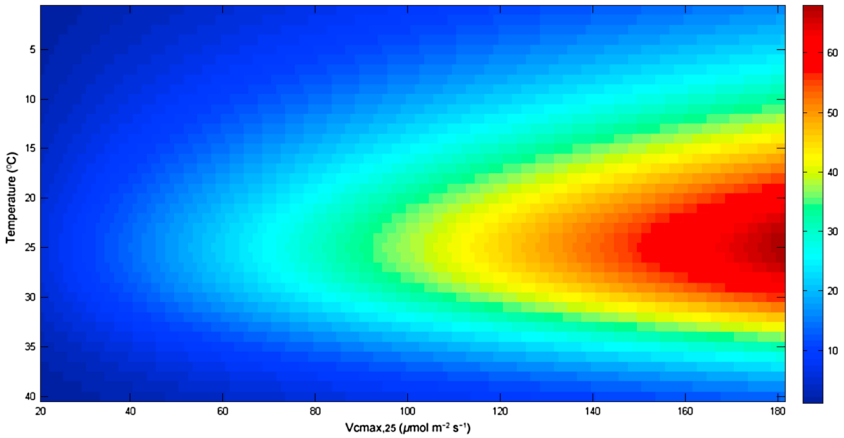

Figure 4. Maximum photosynthetic rate (P_m) distribution map for different temperatures and $V_{cmax,25}$.

once the temperature is above 25°C (Figure 4). For all $V_{cmax,25}$ from 20 to 180 μmol m^{-2} s^{-1}, the P_m all reach its maximum value at 25°C. Therefore, we can deduce that P_m may vary remarkably over the annual period in regions with distinct seasonality, whereas P_m may be kept constant over the annual period in regions without obviously seasonal variations in temperature. With respect to the effect of $V_{cmax,25}$ on P_m, we can see that the P_m value increases linearly with increasing $V_{cmax,25}$ with the maximum P_m occurring at the highest $V_{cmax,25}$. At the same time, the average P_m over the temperature range from 1 to 40°C is also linearly correlated with $V_{cmax,25}$ (Figure 5a). The standard deviation of P_m increases with $V_{cmax,25}$, while the variation coefficients of P_m are almost the same for all $V_{cmax,25}$ with the average value of 43.27% (Figure 5a).

3.2.2. Variations of P_m Across Vegetation Types

Since P_m is linearly correlated with $V_{cmax,25}$, the variation ranges of P_m for different vegetation types depend on those of $V_{cmax,25}$. Among vegetation types [*Kattge et al.*, 2009], the maximum average of P_m is highest for C3 crops, reaching 23.27 μmol m^{-2} s^{-1} with largest SD of 11.38, while the minimum average of P_m is 6.81 μmol m^{-2} s^{-1} for tropical trees (oxisols) with the smallest SD of 3.09 μmol m^{-2} s^{-1} (Table 3). There is nearly a fourfold range in average P_m among different vegetation types. That is because, in these vegetation types, the high P_m value of C3 crops is attributable to the large $V_{cmax,25}$ value and the small P_m value of tropical trees (oxisols) is associated with the small $V_{cmax,25}$ value. The differences in the average values of P_m are very small for temperate evergreen broadleaf and deciduous trees, evergreen needleleaf trees, evergreen shrubs, and deciduous shrubs, with the average value of about 13 μmol m^{-2} s^{-1}, but temperate evergreen broadleaf trees have the largest SD among all vegetation types (Table 3). *Whitehead and Gower* [2001] reported a midsummer peak value of P_m of 12.6 μmol m^{-2} s^{-1} to 15 μmol m^{-2} s^{-1} for a tree species, *Populus tremuloides*, this is consistent with the average P_m of 12.99 μmol m^{-2} s^{-1} for temperate deciduous broadleaf trees found in our study. *Ellsworth et al.* [2004] compared P_m for 16 plant species of herb, tree, and shrub growth forms, and most of their Pm values fall in the range of P_m presented in this study (Table 3).

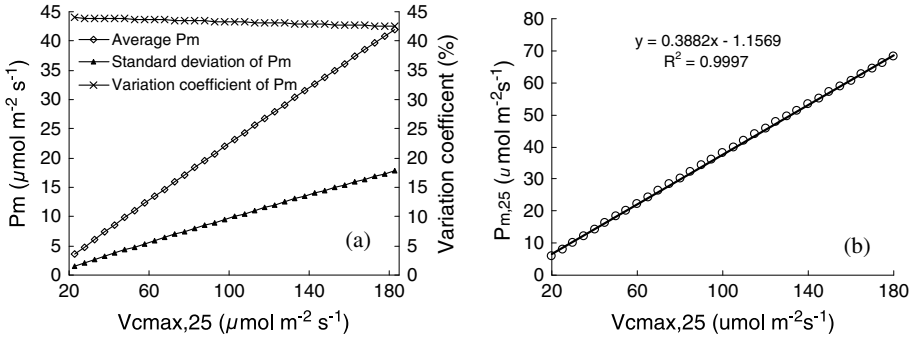

Figure 5. (a) Average, standard deviation, and variation coefficient of P_m for different $V_{cmax,25}$. (b) Relationship between maximum carboxylation velocity at 25°C ($V_{cmax,25}$) and maximum P_m at 25°C($P_{m,25}$).

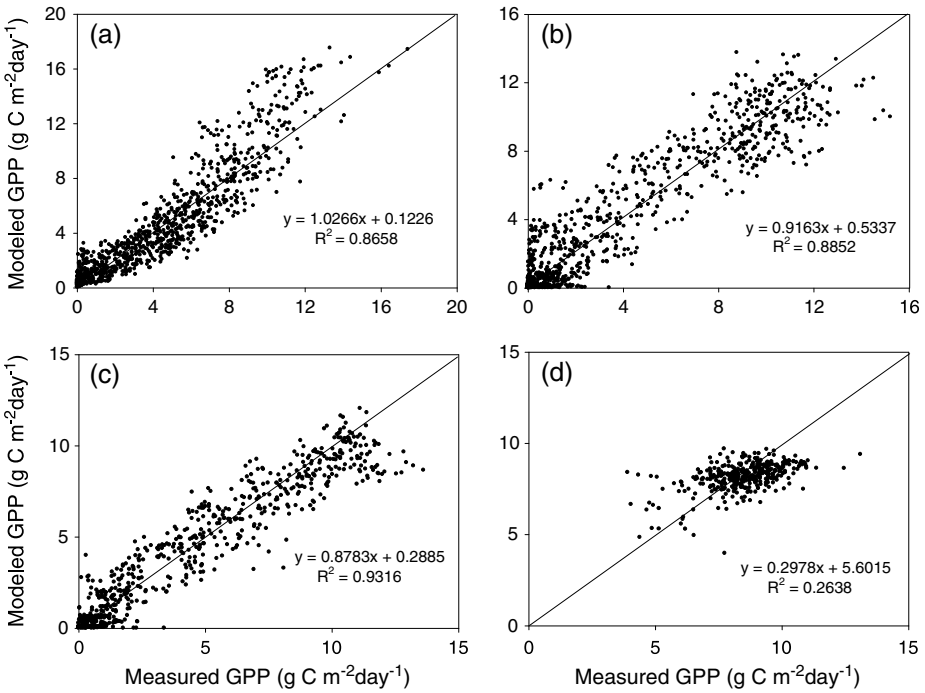

Figure 6. Scatterplots of GPP simulated by the modified rectangular hyperbolic model versus measured GPP for the calibration sites of (a) evergreen needleleaf forest, (b) deciduous broadleaf forest, (c) grassland, and (d) evergreen broadleaf forest. Diagonal lines are the 1:1 lines.

3.2.3. Relationship Between $P_{m,25}$ and $V_{cmax,25}$

Both $V_{cmax,25}$ and maximum P_m at 25°C($P_{m,25}$) are parameters depicting photosynthesis capacity. We found that the $P_{m,25}$ is linearly related to $V_{cmax,25}$ (Figure 5b). $V_{cmax,25}$ is an important parameter in Farquhar's mechanistic photosynthesis model, which is used in process-based GPP models. However, $V_{cmax,25}$ cannot be measured directly but must be inferred by model inversion from photosynthesis measurements [*Kattge et al.*, 2009]. Compared to $V_{cmax,25}$, $P_{m,25}$ has been measured much more frequently under favorable natural conditions. We can infer that $V_{cmax,25}$ can be obtained indirectly from measurements of $P_{m,25}$. Since a number of studies have pointed out that P_m is correlated with leaf nitrogen level [*Sands*, 1995; *Wright et al.*, 2004; *Kattge et al.*, 2009], $P_{m,25}$ could be estimated at large scale using remotely sensed data through establishing the relationship between remote sensing proxies such as vegetation indices and leaf nitrogen content [*Martin et al.*, 2008]. Therefore, it is possible to derive $V_{cmax,25}$ using remotely sensed data at large spatial scales. Here we provide an alternative way to estimate $V_{cmax,25}$.

3.3. Evaluation of Modified RHM Using Measurements

The hourly modeled results are aggregated to daily values, which are used to compare with measured daily GPP (Figure 6). The RMSE and R^2 values of the calibration data set are calculated for all four vegetation types, i.e., ENF, DBF, GRA, and EBF. As seen, for ENF, DBF, and GRA sites, the modeled GPP values agree well with those of measured GPP with the R^2 of 0.87, 0.88, and 0.93 and with the RMSE of 1.71, 1.43, and 1.02 g C m^{-2} d^{-1} for ENF, DBF, and GRA sites, respectively. For EBF site, the modeled and measured GPP shows a bad agreement with R^2 of 0.26. However, given the small variation range of GPP in the tropical evergreen forest, MRHM performs acceptably well in tracing the seasonal variation of GPP with a RMSE of 1.20 g C m^{-2} d^{-1}.

For the validation data set, similar results to calibration data set are obtained for the four vegetation types (Figure 7). The relative large R^2 values are obtained with RMSE of 1.95, 1.81, and 1.39 g C m^{-2} d^{-1} for ENF, DBF, and GRA sites, respectively. The R^2 for EBF site is still small, same to that of calibration set, with a RMSE of 1.71 g C m^{-2} d^{-1}, this may be caused by two possible reasons. One reason is the flaw of the MRHM. Although the MRHM is based on Baldocchi's model, there are still some mechanisms to be explored to

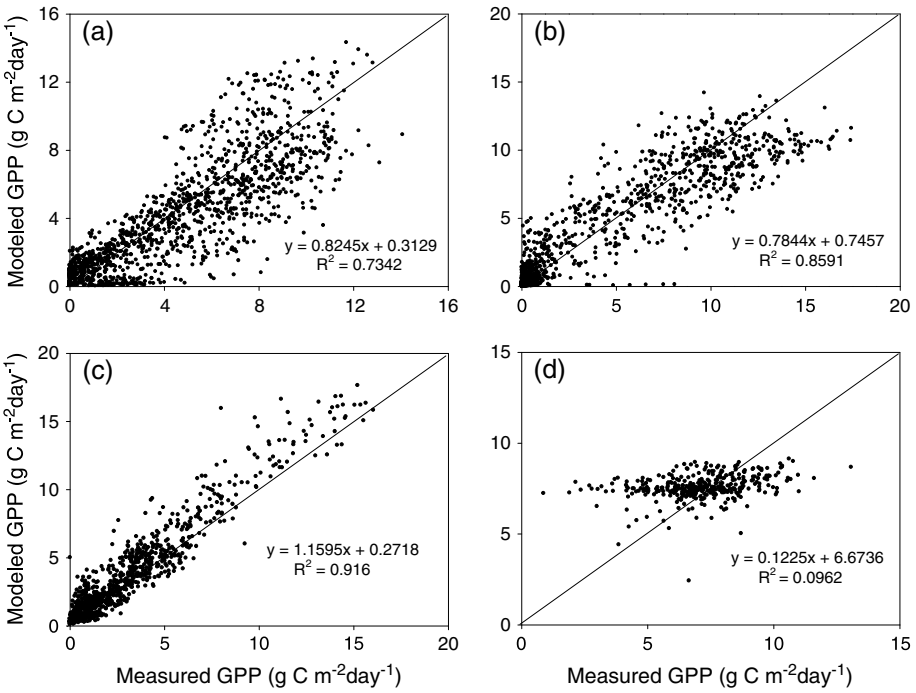

Figure 7. Scatterplots of GPP simulated by the modified rectangular hyperbolic model versus measured GPP for the validation sites of (a) evergreen needleleaf forest, (b) deciduous broadleaf forest, (c) grassland, and (d) evergreen broadleaf forest. Diagonal lines are the 1:1 lines.

improve the ecosystem model capacity because of the complexity of ecosystem processes [*Mo et al*., 2012]. Another reason may come from measurement error, considering the maximum of 30% uncertainty in eddy-covariance measurements [*Anthoni et al*., 2004].

3.4. Comparison Between Modified RHM and BEPS

A process-based model, the BEPS model, is also used to evaluate the performance of modified RHM (MRHM), because the BEPS and the MRHM are both based on the Baldocchi's photosynthesis model [*Baldocchi*, 1994]. Since the same key parameters are used for the two models, the intercomparison between the BEPS model and the MRHM will eliminate the effect of discrepancies between the modeled and measured GPP and explicitly demonstrates whether MRHM has the potential to accurately simulate GPP as a process-based model. The intercomparison results show that the distribution of the data points in Figure 8 is much closer to diagonal lines than those data points in Figures 6 and 7. Simulated daily GPP values from MRHM were regressed on GPP values simulated by the BEPS model for the four vegetation types. Slopes close to 1 and intercepts close to 0 indicate good agreements between the GPP values simulated by MRHM and the BEPS model. However, MRHM tends to slightly underestimate daily GPP compared to the BEPS model for all the four vegetation types (Figure 8), which may be caused by the differences of the two models in considering the effect of humidity on photosynthesis.

A distinct feature of MRHM is that the two parameter, α and P_m, of MRHM vary with temperature. In order to illustrate the importance of temperature adjustments of the two parameters in MRHM, a comparison between a rectangular hyperbolic model without temperature adjustments (RHM-NoTemp, in which the temperature-averaged α and P_m are used), and the BEPS are performed with the GPP values from the BEPS as the standard data (Figure 9). The results show RHM-NoTemp either overestimates or underestimates daily GPP, depending on temperature values used for the simulation. If the temperature was higher than the temperature corresponding to the temperature-averaged α or Pm and lower than 25°C, then the GPP by RHM-NoTemp would be underestimated, and vice versa. From the Figure 9, we can see that the data points are deviated from the diagonal lines and are far more scattered than those in Figure 8 although the relatively large R^2 are obtained for all four vegetation types.

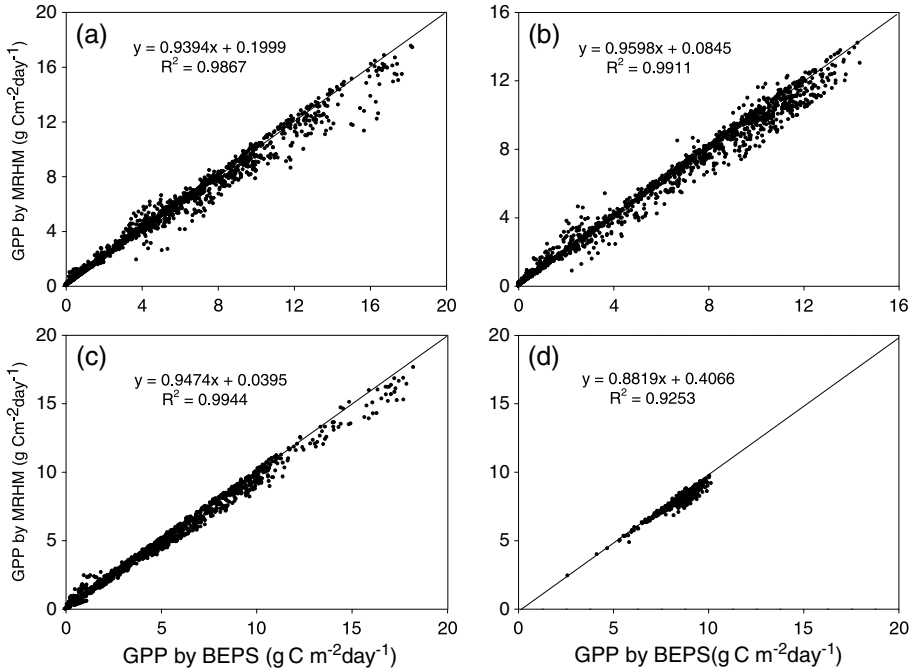

Figure 8. Scatterplots of GPP simulated by the modified rectangular hyperbolic model versus GPP by BEPS model for the vegetation types of (a) evergreen needleleaf forest, (b) deciduous broadleaf forest, (c) grassland, and (d) evergreen broadleaf forest. Diagonal lines are the 1:1 lines.

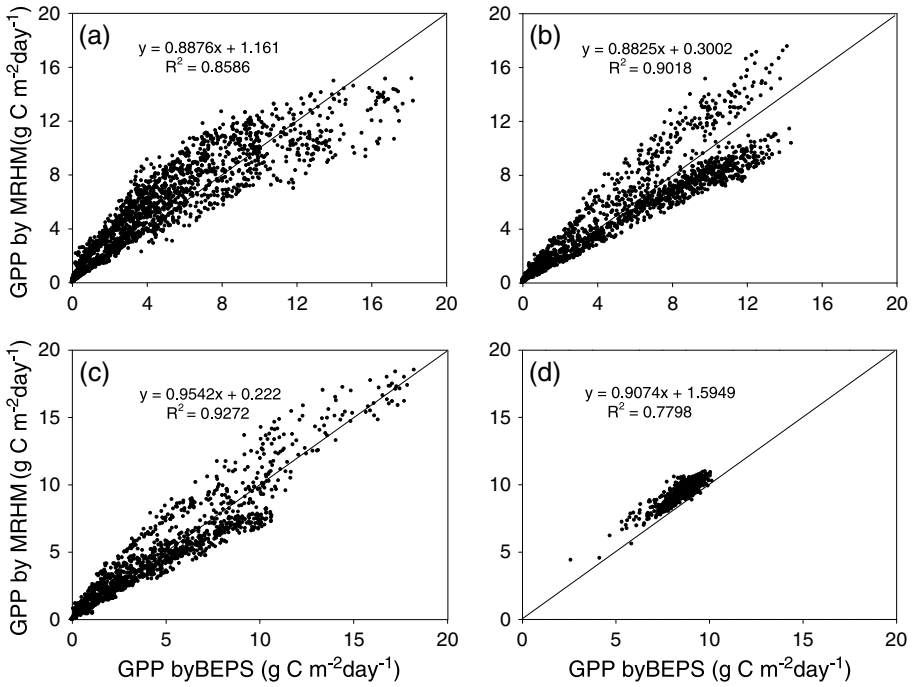

Figure 9. Scatterplots of GPP simulated by the modified rectangular hyperbolic model with temperature-averaged α and P_m versus GPP by BEPS model for the vegetation types of (a) evergreen needleleaf forest, (b) deciduous broadleaf forest, (c) grassland, and (d) evergreen broadleaf forest. Diagonal lines are the 1:1 lines.

4. Discussion

4.1. Improvement of Modified RHM Over Traditional RHM

Traditional RHM is usually used by keeping the two parameters, α and P_m, constant or through fitting RHM for a period of time such as a week, 10 days or a month and so on, in which temperatures varies in small ranges and hence is assumed to be constant. *Saito et al*. [2005] divided the 2002 growing season of rice into 23 periods, and determined α and P_m for the respective periods by fitting a rectangular hyperbolic function of incident PAR against GPP using the least squares method. *Yan et al*. [2009] applied a traditional RHM to a period of 10 days. *Kanniah et al*. [2013] estimated α and P_m on a monthly basis. These procedures were laborious and time consuming, and the derived α and P_m were data set dependent. The reason they made these partitions for a growing season is that the α and P_m are variable for different temperatures and vegetation types, as *Ide et al*. [2010] reported that α and P_m show clear seasonal changes accompanying phenological stages. In the study, we present a modified temperature- and vegetation-type-adapted MRHM, which can dynamically determine the α and P_m according to environmental conditions when MRHM is applied. Therefore, the MRHM overcomes the weakness of traditional RHMs.

In addition, traditional RHMs usually treat the canopy as a big leaf, while the MRHM is based on a two-leaf model, separating a canopy into sunlit and shaded leaf groups. Previous studies have proved that big-leaf models may incorrectly estimate canopy GPP [*Sprintsin et al*., 2012] and fail to simulate its day-to-day variations [*Chen et al*., 1999], because the quantum response of leaf photosynthesis is nonlinear and the use of mean absorbed radiation in the big-leaf model will significantly overestimate the canopy photosynthesis [*Wang and Leuning*, 1998], due to the variable large contribution from the shaded leaves. The two-leaf approach is successful because it applies the separation of incoming radiation into its direct and diffuse portions and considers the differences in APARs for sunlit and shaded leaves.

4.2. Limitation of the Modified RHM

Although RHM is an empirical model, the MRHM has the gene of Farquhar's mechanistic model by establishing the relationship between α-P_m and $V_{cmax,25}$-temperature. It means that the effects of radiation and temperature on GPP with consideration of the underlying biological mechanisms have been included in the MRHM. However, the VPD effect on GPP is based on an empirical function from Moderate Resolution Imaging Spectroradiometer GPP algorithm, although including the VPD effect in the MRHM improves the modeled GPP derived from the hyperbolic light response curve.

In this study, soil moisture is not taken into account, so under the condition of very dry season, the method proposed here may incur considerable errors in GPP estimation. A possible solution to the problem is to introduce a soil water scalar into the MRHM by considering the soil water effect on GPP as some studies did. *Vourlitis et al*. [2004] used a logistic function of relative water content to consider the effect of water availability on GPP estimation. A previous study has found that water indices that are based on near-infrared and shortwave-infrared bands are sensitive to changes in equivalent water thickness at leaf and canopy levels [*Ceccato et al*., 2001]. So in some studies, water indices derived from remote sensing data were employed to construct a downregulation function to reduce GPP under conditions of deficient soil water content [*Xiao et al*., 2005; *Wu et al*., 2010].

5. Conclusions

In this study, we present a two-leaf rectangular hyperbolic model for estimating GPP across vegetation types and climate conditions. The model is build by coupling a modified RHM with a two-leaf strategy. The MRHM is established by linking a rectangular hyperbolic model with a variant of Farquhar's model, i.e., Baldocchi's model, to obtain the two parameters, α and P_m, as functions of temperature and $V_{cmax,25}$. We found that α is almost invariant among different vegetation types under the same temperature conditions, whereas it decreases with increasing of temperature from 1 to 40°C for a given $V_{cmax,25}$. P_m varies not only with temperature but also with vegetation types with different $V_{cmax,25}$. For a given vegetation type, it usually increases with increasing temperature, reaches its maximum values at 25°C, and then it decreases sharply with further increase in temperature. The maximum P_m at 25°C is highly linearly correlated with V_{cmax} at 25°C, making their mutual conversion possible.

The dynamic use of α and P_m according to temperature and $V_{cmax,25}$ in the MRHM can be expected to substantially reduce the large uncertainty in GPP estimation using traditional RHMs. Twenty-two CO_2 eddy-covariance sites with four different vegetation types, i.e., evergreen needleleaf forest, deciduous broadleaf forest, grassland, evergreen broadleaf forest, and a process-based model (BEPS model) are used to evaluate the MRHM for GPP estimation. For daily GPP simulation, the MRHM explains 87%, 88%, and 93% of daily GPP variance with RMSE of 1.71, 1.43, and 1.02 g C m^{-2} d^{-1} for ENF, DBF, and GRA sites, respectively. For EBF site, the R^2 value is only 0.26 with a RMSE of 1.20 g C m^{-2} d^{-1} due to the small dynamic range of GPP. As to the comparison between MRHM and the BEPS model, the good agreements between the simulated GPP values derived from MRHM and the BEPS model were proved by the high R^2 values that nearly equal 1, and low intercepts of regression equations that close to 0. The comparisons of the simulated GPP using the MRHM with the measured and BEPS modeled GPP demonstrate that the MRHM can simulate GPP as accurately as process-based model and in the meantime with the advantage of simplicity as LUE model. Therefore, the MRHM can be expected to integrate with temporally continuous and spatially extensive satellite data to monitor GPP dynamic at large scale.

Acknowledgments

This study is supported by the Natural Science Foundation of China (51109183, 41371393), the Specialized Research Fund for the Doctoral Program of Higher Education of China (20110101120036), and the opening foundation of Institute of Remote Sensing and Earth Sciences, Hangzhou Normal University (PDKF2011YG03). We thank the Fluxnet-Canada and AmeriFlux networks, the site principal investigators, participants, and data collection and processing staff for the tower flux data used in this study.

References

Allison, V. J., R. M. Miller, J. D. Jastrow, R. Matamala, and D. R. Zak (2005), Changes in soil microbial community structure in a tallgrass prairie chronosequence, *Soil Sci. Soc. Am. J.*, *69*(5), 1412–1421, doi:10.2136/sssaj2004.0252.

Anthoni, P. M., A. Freibauer, O. Kolle, and E. Schulze (2004), Winter wheat carbon exchange in Thuringia, Germany, *Agric. For. Meteorol.*, *121*, 55–67, doi:10.1016/S0168-1923(03)00162-X.

Baldocchi, D. (1994), An analytical solution for coupled leaf photosynthesis and stomatal conductance models, *Tree Physiol.*, *14*, 1069–1079, doi:10.1093/treephys/14.7-8-9.1069.

Baldocchi, D., et al. (2001), Fluxnet: A new tool to study the temporal and spatial variability of ecosystem-scale carbon dioxide, water vapor, and energy flux densities, *Bull. Am. Meteorol. Soc.*, *82*, 2415–2434, doi:10.1175/1520-0477(2001)082<2415:FANTTS>2.3.CO;2.

Baldocchi, D. D. (2003), Assessing the eddy covariance technique for evaluating carbon dioxide exchange rates of ecosystems: Past, present and future, *Global Change Biol.*, *9*(4), 479–492, doi:10.1046/j.1365-2486.2003.00629.x.

Ball, J. T. (1988), An analysis of stomatal conductance, PhD thesis, Stanford University, 89.

Barr, A. G., T. A. Black, E. H. Hogg, N. Kljun, K. Morgenstern, and Z. Nesic (2004), Inter-annual variability in the leaf area index of a boreal aspen-hazelnut forest in relation to net ecosystem production, *Agric. For. Meteorol.*, *126*, 237–255, doi:10.1016/j.agrformet.2004.06.011.

Ceccato, P., N. Gobron, S. Flasse, B. Pinty, and S. Tarantola (2001), Designing a spectral index to estimate vegetation water content from remote sensing data: Part 1. Theoretical approach, *Remote Sens. Environ.*, *82*, 188–197, doi:10.1016/S0034-4257(02)00037-8.

Chen, B., J. M. Chen, and W. Ju (2007), Remote sensing-based ecosystem-atmosphere simulation scheme (EASS)–Model formulation and test with multiple-year data, *Ecol. Modell.*, *209*, 277–300, doi:10.1016/j.ecolmodel.2007.06.032.

Chen, B., T. A. Black, N. C. Coops, and T. Hilker (2009), Assessing tower flux footprint climatology and scaling between remotely sensed and eddy covariance measurements, *Boundary Layer Meteorol.*, *130*, 137–167, doi:10.1007/s10546-008-9339-1.

Chen, J. M., G. Mo, J. Pisek, J. Liu, F. Deng, M. Ishizawa, and D. Chan (2012), Effects of foliage clumping on the estimation of global terrestrial gross primary productivity, *Global Biogeochem. Cycles*, *26*, GB1019, doi:10.1029/2010GB003996.

Chen, J. M., J. Liu, J. Cihlar, and M. L. Goulden (1999), Daily canopy photosynthesis model through temporal and spatial scaling for remote sensing applications, *Ecol. Modell.*, *124*, 99–119, doi:10.1016/S0304-3800(99)00156-8.

Cook, B. D., et al. (2004), Carbon exchange and venting anomalies in an upland deciduous forest in northern Wisconsin, USA, *Agric. For. Meteorol.*, *126*, 271–295, doi:10.1016/j.agrformet.2004.06.008.

Coops, N. C., C. J. Ferster, R. H. Waring, and J. A. Nightingale (2009), Comparison of three models for predicting gross primary production across and within forested ecoregions in the contiguous United States, *Remote Sens. Environ.*, *113*, 680–690, doi:10.1016/j.rse.2008.11.013.

Curtis, P. S., P. J. Hanson, P. Bolstad, C. Barford, J. C. Randolph, H. P. Schmid, and K. B. Wilson (2002), Biometric and eddy-covariance based estimates of annual carbon storage in five eastern North American deciduous forests, *Agric. For. Meteorol.*, *113*, 3–19, doi:10.1016/S0168-1923(02)00099-0.

Dore, S., T. E. Kolb, M. Montes-Helu, S. E. Eckert, B. W. Sullivan, B. A. Hungate, J. P. Kaye, S. C. Hart, G. W. Koch, and A. Finkral (2010), Carbon and water fluxes from ponderosa pine forests disturbed by wildfire and thinning, *Ecol. Appl.*, *20*(3), 663–683, doi:10.1890/09-0934.1.

Ellsworth, D. S., P. B. Reich, E. S. Naumburg, G. W. Koch, M. E. Kubiske, and S. Smith (2004), Photosynthesis, carboxylation and leaf nitrogen responses of 16 species to elevated pCO2 across four free-air CO2 enrichment experiments in forest, grassland and desert, *Global Change Biol.*, *10*, 2121–2138, doi:10.1111/j.1365-2486.2004.00867.x.

Falk, M., S. Wharton, M. Schroeder, S. Ustin, and K. T. Paw U (2008), Flux partitioning in an old-growth forest: Seasonal and interannual dynamics, *Tree Physiol.*, *28*, 509–520.

Farquhar, G. D., S. von Caemmerer, and J. A. Berry (1980), A biochemical model of photosynthetic CO2 assimilation in leaves of C3 species, *Planta*, *149*, 78–90, doi:10.1007/BF00386231.

Goulden, M. L., S. D. Miller, and H. R. da Rocha (2006), Nocturnal cold air drainage and pooling in a tropical forest, *J. Geophys. Res.*, *111*, D08S04, doi:10.1029/2005JD006037.

Groenendijk, M., A. J. Dolman, and C. Ammann (2011), Seasonal variation of photosynthetic model parameters and leaf area index from global Fluxnet eddy covariance data, *J. Geophys. Res.*, *116*, G04027, doi:10.1029/2011JG001742.

Gu, L., et al. (2007), Influences of biomass heat and biochemical energy storages on the land surface fluxes and diurnal temperature range, *J. Geophys. Res.*, *112*, D02107, doi:10.1029/2006JD007425.

He, M., et al. (2013), Development of a two-leaf light use efficiency model for improving the calculation of terrestrial gross primary productivity, *Agric. For. Meteorol.*, *173*, 28–39, doi:10.1016/j.agrformet.2013.01.003.

Hilker, T., N. C. Coops, M. A. Wulder, T. A. Black, and R. D. Guy (2008), The use of remote sensing in light use efficiency based models of gross primary production: A review of current status and future requirements, *Sci. Total Environ.*, *404*, 411–423, doi:10.1016/j.scitotenv.2007.11.007.

Hollinger, D. Y., et al. (2004), Spatial and temporal variability in forest-atmosphere CO2 exchange, *Global Change Biol.*, *10*, 1689–1706.

Ide, R., T. Nakaji, and H. Oguma (2010), Assessment of canopy photosynthetic capacity and estimation of GPP by using spectral vegetation indices and the light-response function in a larch forest, *Agric. For. Meteorol.*, *150*, 389–398, doi:10.1016/j.agrformet.2009.12.009.

Jassal, R. S., T. A. Black, D. L. Spittlehouse, C. Brümmer, and Z. Nesic (2009), Evapotranspiration and water use efficiency in different-aged Pacific Northwest Douglas-fir stands, *Agric. For. Meteorol.*, *149*, 1168–1178, doi:10.1016/j.agrformet.2009.02.004.

Jenkins, J. P., A. D. Richardson, B. H. Braswell, S. V. Ollinger, D. Y. Hollinger, and M. L. Smith (2007), Refining light-use efficiency calculations for a deciduous forest canopy using simultaneous tower-based carbon flux and radiometric measurements, *Agric. For. Meteorol.*, *143*, 64–79, doi:10.1016/j.agrformet.2006.11.008.

Ju, W., J. M. Chen, T. A. Black, A. G. Barr, J. Liu, and B Chen (2006), Modelling multi-year coupled carbon and water fluxes in a boreal aspen forest, *Agric. For. Meteorol.*, *140*, 136–151, doi:10.1016/j.agrformet.2006.08.008.

Kanniah, K. D., J. Beringer, and L. Hutley (2013), Exploring the link between clouds, radiation, and canopy productivity of tropical savannas, *Agric. Forest Meteorol.*, doi:10.1016/j.agrformet.2013.06.010.

Kattge, J., W. Knorr, T. Raddatz, and C. Wirth (2009), Quantifying photosynthetic capacity and its relationship to leaf nitrogen content for global-scale terrestrial biosphere models, *Global Change Biol.*, *15*, 976–991, doi:10.1111/j.1365-2486.2008.01744.x.

Krishnan, P., T. P. Meyers, R. L. Scott, L. Kennedy, and M. Heuer (2012), Energy exchange and evapotranspiration over two temperate semi-arid grasslands in North America, *Agric. For. Meteorol.*, *153*, 31–44, doi:10.1016/j.agrformet.2011.09.017.

Law, B. E., R. H. Waring, P. M. Anthoni, and J. D. Aber (2000), Measurements of gross and net ecosystem productivity and water vapour exchange of a Pinus ponderosa ecosystem, and an evaluation of two generalized models, *Global Change Biol.*, *6*, 155–168, doi:10.1046/j.1365-2486.2000.00291.x.

Leuning, R., F. M. Kelliher, D. G. G. de Pury, and E. D. Schulze (1995), Leaf nitrogen, photosynthesis, conductance and transpiration: Scaling from leaves to canopy, *Plant, Cell Environ.*, *18*, 1183–1200.

Liu, J., J. M. Chen, J. Cihlar, and W. M. Park (1997), A process-based boreal ecosystem productivity simulator using remote sensing inputs, *Remote Sens. Environ.*, *62*, 158–175, doi:10.1016/S0034-4257(97)00089-8.

Martin, M. E., L. C. Plourde, S. V. Ollinger, M.-L. Smith, and B. E. McNeil (2008), A generalizable method for remote sensing of canopy nitrogen across a wide range of forest ecosystems, *Remote Sen. Environ.*, *112*, 3511–3519, doi:10.1016/j.rse.2008.04.008.

Mo, X., S. Liu, and Z. Lin (2012), Evaluation of an ecosystem model for a wheat maize double cropping system over the North China Plain, *Environ. Modell. Software*, *32*, 61–73, doi:10.1016/j.envsoft.2011.07.002.

Monson, R. K., J. P. Sparks, T. N. Rosenstiel, L. E. Scott-Denton, T. E. Huxman, P. C. Harley, A. A. Turnipseed, S. P. Burns, B. Backlund, and J. Hu (2005), Climatic influences on net ecosystem CO2 exchange during the transition from wintertime carbon source to springtime carbon sink in a high-elevation, subalpine forest, *Oecologia*, *146*, 130–147.

Monteith, J. L. (1972), Solar radiation and production in tropical ecosystems, *J. Appl. Ecol.*, *9*, 747–766, doi:10.2307/2401901.

Norman, J. M. (1982), Simulation of microclimates, in *Biometeorology in Integrated Pest Management*, edited by J. L. Hatfield and I. J. Thomason, pp. 65–99, Academic Press, New York.

Oren, R., C. I. Hseih, P. Stoy, J. Albertson, H. R. McCarthy, P. Harrell, and G. G. Katul (2006), Estimating the uncertainty in annual net ecosystem carbon exchange: Spatial variation in turbulent fluxes and sampling errors in eddy-covariance measurements, *Global Change Biol.*, *12*(5), 883–896, doi:10.1111/j.1365-2486.2006.01131.x.

Pachepsky, L. B., J. D. Haskett, and B. Acock (1996), An adequate model of photosynthesis—I. Parameterization, validation and comparison of models, *Agric. Syst.*, *50*, 209–225, doi:10.1016/0308-521X(94)00051-R.

Papale, D., and A. Valentini (2003), A new assessment of European forests carbon exchange by eddy fluxes and artificial neural network spatialization, *Glob. Change Biology*, *9*, 525–535.

Payeur-Poirier, J.-L., C. Coursolle, H. A. Margolis, and M.-A. Giasson (2012), CO2 fluxes of a boreal black spruce chronosequence in eastern North America, *Agric. For. Meteorol.*, *153*, 94–105, doi:10.1016/j.agrformet.2011.07.009.

Potter, C. B., J. T. Randerson, C. B. Field, P. A. Matson, P. M. Vitousek, H. A. Mooney, and S. A. Klooster (1993), Terrestrial ecosystem production: A process model based on global satellite and surface data, *Global Biogeochem. Cycle*, *7*, 811–841, doi:10.1029/93GB02725.

Prince, S. D., and S. N. Goward (1995), Global primary production: A remote sensing approach, *J. Biogeogr.*, *22*, 815–835, doi:10.2307/2845983.

Richardson, A. D., and D. Y. Hollinger (2005), Statistical modeling of ecosystem respiration using eddy covariance data: Maximum likelihood parameter estimation, and Monte Carlo simulation of model and parameter uncertainty, applied to three simple models, *Agric. For. Meteorol.*, *131*(3–4), 191–208, doi:10.1016/j.agrformet.2005.05.008.

Running, S. W., R. R. Nemani, F. A. Heinsch, M. Zhao, M. Reeves, and H. Hashimoto (2004), A continuous satellite-derived measure of global terrestrial primary production, *BioScience*, *54*, 547–560, doi:10.1641/0006-3568(2004)054[0547:ACSMOG]2.0.CO;2.

Saito, M., A. Miyata, H. Nagai, and T. Yamada (2005), Seasonal variation of carbon dioxide exchange in rice paddy field in Japan, *Agric. For. Meteorol.*, *135*, 93–109, doi:10.1016/j.agrformet.2005.10.007.

Sands, P. J. (1995), Modelling canopy production. II. From single-leaf photosynthetic parameters to daily canopy photosynthesis, *Aust. J. Plant Physiol.*, *22*, 603–614, doi:10.1071/PP9950603.

Schmid, H. P., C. S. B. Grimmond, F. Cropley, B. Offerle, and H. B. Su (2000), Measurements of CO2 and energy fluxes over a mixed hardwood forest in the mid-western United States, *Agric. For. Meteorol.*, *103*, 357–374, doi:10.1016/S0168-1923(00)00140-4.

Sprintsin, M., J. M. Chen, A. Desai, and C. M. Gough (2012), Evaluation of leaf-to-canopy upscaling methodologies against carbon flux data in North America, *J. Geophys. Res.*, *117*, G01023, doi:10.1029/2010JG001407.

Suyker, A. E., S. B. Verma, G. G. Burba, T. J. Arkebauer, D. T. Walters, and K. G. Hubbard (2004), Growing season carbon dioxide exchange in irrigated and rainfed maize, *Agric. For. Meteorol.*, *124*, 1–13, doi:10.1016/j.agrformet.2004.01.011.

Urbanski, S., C. Barford, S. Wofsy, C. Kucharik, E. Pyle, J. Budney, K. McKain, D. Fitzjarrald, M. Czikowsky, and J. W. Munger (2007), Factors controlling CO2 exchange on timescales from hourly to decadal at Harvard Forest, *J. Geophys. Res.*, *112*, G02020, doi:10.1029/2006JG000293.

Vourlitis, G. L., G. L. Vourlitis, N. P. Filho, M. M. S. Hayashi, J. d. S. Nogueira, F. Raiter, W. Hoegel, and J. H. Campelo Jr. (2004), Effects of meteorological variations on the CO2 exchange of a Brazilian transitional tropical forest, *Ecol. Appl.*, *14*, 89–100, doi:10.1890/01-6005.

Wang, Y. P., and R. Leuning (1998), A two-leaf model for canopy conductance, photosynthesis and partitioning of available energy. I: Model description and comparison with a multi-layered model, *Agric. For. Meteorol.*, *91*, 89–111, doi:10.1016/S0168-1923(98)00061-6.

Whitehead, D., and S. T. Gower (2001), Photosynthesis and light-use efficiency by plants in a Canadian boreal forest ecosystem, *Tree Physiol.*, *21*, 925–929, doi:10.1093/treephys/21.12-13.925.

Wick, B., E. Veldkamp, W. Z. de Mello, M. Keller, and P. Crill (2005), Nitrous oxide fluxes and nitrogen cycling along a pasture chronosequence in Central Amazonia, Brazil, *Biogeosciences*, *2*, 175–187, doi:10.5194/bg-2-175-2005.

Wilson, T. B., and T. P. Meyers (2007), Determining vegetation indices from solar and photosynthetically active radiation fluxes, *Agric. For. Meteorol.*, *144*, 160–179, doi:10.1016/j.agrformet.2007.04.001.

Wright, I. J., et al. (2004), The worldwide leaf economics spectrum, *Nature*, *428*, 821–827, doi:10.1038/nature02403.

Wu, C., J. W. Munger, Z. Niu, and D. Kuang (2010), Comparison of multiple models for estimating gross primary production using MODIS and eddy covariance data in Harvard Forest, *Remote Sens. Environ.*, *114*, 2925–2939, doi:10.1016/j.rse.2010.07.012.

Xiao, X. M. (2006), Light absorption by leaf chlorophyll and maximum light use efficiency, *IEEE Trans. Geosci. Remote*, *44*, 1933–1935, doi:10.1109/TGRS.2006.874796.

Xiao, X. M., Q. Y. Zhang, D. Hollinger, J. Aber, and B. Moore (2005), Modeling gross primary production of an evergreen needleleaf forest using MODIS and climate data, *Ecol. Appl.*, *15*, 954–969, doi:10.1890/04-0470.

Yan, H., Y. Fu, X. Xiao, H. Q. Huang, H. He, and L. Ediger (2009), Modeling gross primary productivity for winter wheat–maize double cropping system using MODIS time series and CO2 eddy flux tower data, *Agric. Ecosyst. Environ.*, *129*, 391–400, doi:10.1016/j.agee.2008.10.017.

Yang, Y., S. Shang, H. Guan, and L. Jiang (2013), A novel algorithm to assess gross primary production for terrestrial ecosystems from MODIS imagery, *J. Geophys. Res. Biogeosci.*, *118*, 590–605, doi:10.1002/jgrg.20056.

Zhang, F., J. M. Chen, J. Chen, C. M. Gough, T. A. Martin, and D. Dragoni (2012), Evaluating spatial and temporal patterns of MODIS GPP over the conterminous U.S. against flux measurements and a process model, *Remote Sens. Environ.*, *124*, 717–729, doi:10.1016/j.rse.2012.06.023.